International Journal of Multiphase Flow 34 (2008) 1130–1141

Contents lists available at ScienceDirect

International Journal of Multiphase Flow

journal homepage: www.elsevier.com/locate/ijmulflow

Bubbly jets in stagnant water

Iran E. Lima Neto, David Z. Zhu *, Nallamuthu Rajaratnam

Department of Civil and Environmental Engineering, University of Alberta, NREF Building, Edmonton AB, Canada T6G 2W2

ARTICLE INFO

Article history:
Received 16 April 2008
Received in revised form 9 June 2008
Accepted 27 June 2008
Available online 6 July 2008

ABSTRACT

Air–water bubbly jets are studied experimentally in a relatively large water tank with a gas volume fraction, C_o, of up to 80% and nozzle Reynolds number, *Re*, ranging from 3500 to 17,700. Measurements of bubble properties and mean axial water velocity are obtained and two groups of experiments are identified, one with relatively uniform bubble sizes and another with large and irregular bubbles. For the first group, dimensionless relationships are obtained to describe bubble properties and mean liquid flow structure as functions of C_o and *Re*. Measurements of bubble slip velocity and estimates of the drag coefficient are also provided and compared to those for isolated bubbles from the literature. The study confirms the importance of bubble interactions to the dynamics of bubbly flows. Bubble breakup processes are also investigated for bubbly jets. It was found that a nozzle Reynolds number larger than 8000 is needed to cause breakup of larger bubbles into smaller bubbles and to produce a more uniform bubble size distribution. Moreover, the Weber number based on the mean water velocity appears to be a better criteria than the Weber number based on the bubble slip velocity to describe the onset of bubble breakup away from the nozzle, which occurs at a Weber number larger than 25.

1. Introduction

Two-phase flows such as bubble plumes and bubbly jets have attracted significant interest because of their high benefit–cost ratio for promoting artificial aeration, circulation and mixing in liquids (Iguchi et al., 1997; Morchain et al., 2000; Socolofsky, 2001; Buscaglia et al., 2002; Sahoo and Luketina, 2003; Schierholz et al., 2006; Lima Neto et al., 2007). Bubble plumes are produced by injecting gas in liquids while bubbly jets, which are the focus of this work, are produced by combining liquid pumping with gas pumping. The gas volume fraction in such bubbly jets, defined as the ratio of the gas flow rate to the total gas–liquid mixture flow rate at the nozzle, usually ranges from about 5% to 80%. Previous experimental investigations on the structure of gas–liquid bubbly jets have been conducted by Sun and Faeth (1986a,b), Kumar et al. (1989), and Iguchi et al. (1997). Sun and Faeth (1986a,b) studied air–water bubbly jets with gas volume fractions lower than 10%, where the liquid phase properties were not strongly affected by inter-phase transport. On the other hand, Kumar et al. (1989) and Iguchi et al. (1997) conducted experiments on air–water bubbly jets with gas volume fractions of up to 20% and 50%, respectively, and found that increases in the gas volume fraction slightly increased the mean liquid velocity but significantly increased its turbulent components. However, these experimental investigations were performed in small-scale vessels, with a diameter (or width) of up to 20 cm and a water depth of up to 40 cm, where the tank walls could impact on the behavior of the bubbly jets (as observed by Lima Neto et al. (2008) in bubble plumes). Besides, gas-phase properties in those bubbly jets such as bubble size distribution and bubble velocity have not been investigated in details.

Concerning the effect of bubbles in flows other than bubbly jets, Leitch and Baines (1989) performed experiments on very dilute bubble plumes in a water tank and concluded that the individual bubble wakes can contribute significantly to the entrainment into the liquid jet, in contrast with the results obtained by Kumar et al. (1989) and Iguchi et al. (1997). In this case, since the space between the bubbles was rather large compared to their size and wakes, bubble properties such as relative velocity between the bubbles and the water (i.e., bubble slip velocity) and drag coefficient were assumed to be the same as those for isolated bubbles. However, this is not expected to be true when the space between the bubbles is small, since the interactions of the bubbles and their wakes here have a much greater bearing. Ruzicka (2000) summarized several studies on bubbles rising in line and showed that bubble slip velocity increases and drag coefficient decreases as the space between the bubbles decreases. This trend has also been observed experimentally by Krishna et al. (1999) in bubble columns with large bubble swarms and by Simonnet et al. (2007) in bubble columns with smaller bubbles but with void fractions exceeding a limit of about 15%. Numerical simulations of the

* Corresponding author. Tel.: +1 780 492 5813; fax: +1 780 492 0249.
E-mail addresses: limaneto@ualberta.ca (I.E. Lima Neto), david.zhu@ualberta.ca (D.Z. Zhu), nrajaratnam@ualberta.ca (N. Rajaratnam).

0301-9322/$ - see front matter © 2008 Elsevier Ltd. All rights reserved.
doi:10.1016/j.ijmultiphaseflow.2008.06.005

flow in bubbly suspensions also confirmed this trend (see Sankaranarayanan et al., 2002). Risso and Ellingsen (2002) conducted experiments in a dilute bubble column with local void fractions of up to about 1% and showed that liquid velocity fluctuations are controlled by non-linear interactions between the wakes of the bubbles. Rensen et al. (2005) carried out experiments in a water tunnel with void fractions of up to about 3% and showed that the bubbles cause a more significant turbulent energy enhancement on small scales than on large scales. On the other hand, there is no consensus as to the behavior of bubble slip velocity and drag coefficient as well as liquid flow structure in unconfined bubbly flows such as bubbly jets and bubble plumes in water.

Another complication in bubbly flows is the occurrence of bubble breakup processes, which determine the size of the largest bubbles present in the flow. Bubble breakup is usually assumed to occur when the total shear stress imposed by the liquid overcomes the surface tension, or when the turbulent eddies in the surrounding flow are of comparable sizes of the bubbles and contain enough energy to cause breakup (see Hinze, 1955; Clift et al., 1978). Alternatively, Sevik and Park (1973) and Risso and Fabre (1998) suggested that bubble breakup also depends on the residence time of the bubbles in the turbulent flow field and it can also occur due to a resonance oscillation mechanism. The studies above have been limited, however, to the simple case of isolated bubbles.

In the present study, we conduct experiments in a relatively large tank in order to investigate the behavior of bubbly jets with gas volume fractions ranging from about 5% to 83% and Reynolds numbers at the nozzle exit ranging from about 3500 to 17,700 produced using different nozzles. The objective is to clarify the effect of these two parameters on the properties of the bubbles and the mean liquid flow structure induced by unconfined bubbly jets, as well as to obtain information such as bubble slip velocity, drag coefficient and bubble breakup processes in such two-phase flows. The results from this investigation can be applied to several cases of gas–liquid bubbly flows such as artificial aeration, circulation and mixing in large tanks and water bodies, and can be used for evaluation and validation of CFD models. It is important to note that in this work all the experiments were conducted using tap water. To consider the effect of surfactants on bubbly flows, the reader may refer to Clift et al. (1978) and Rosso and Stenstrom (2006).

2. Experimental apparatus and program

The experiments were performed in a square glass-walled tank with a width of 1.2 m and a height of 0.8 m, shown schematically in Fig. 1. The tank was filled with tap water to a depth of 0.76 m. The gas supply was taken from an air line, while the water was pumped from a small reservoir, and both air and water temperatures were fixed at about 20 °C. Volumetric flow rates of air, Q_{ao}, and water, Q_{wo}, were adjusted by rotameters; mixed into a Venturi injector (Model 484, Mazzei Injector Corporation) connected to a vertical pipe below the tank with a diameter of 25.4 mm; and then discharged through single orifice nozzles of 4, 6, 9 and 13.5 mm in diameter, d_o. A pressure-regulating valve was used to keep the air pressure at 1 atm and ensure a constant air flow rate to the nozzles. The nozzles were placed at the center of the tank with their exit 45 mm above the bottom. The above arrangement ensured bubbly flow conditions at the nozzle entrance for all experiments (see gas–liquid flow regime maps in Oddie and Pearson, 2004) and allowed us to reach gas volume fractions of up to 83%. Table 1 summarizes the experimental conditions, where C_o and Re represent the gas volume fraction and Reynolds number, respectively, at the nozzle:

$$C_o = Q_{ao}/(Q_{ao} + Q_{wo}) \quad (1)$$

$$Re = U_{wo} d_o / \nu_w \quad (2)$$

where U_{wo} is the superficial water velocity based on Q_{wo} and d_o, and ν_w is the kinematic viscosity of water.

Typical images of the bubbles for each experimental condition are depicted in Fig. 2. The first three rows show images for the tests with d_o = 6 mm at constant water flow rate, air flow rate and gas volume fraction, respectively. The last three rows show, respectively, images for the tests with d_o = 4, 9 and 13.5 mm at different flow conditions. A 500 W halogen lamp was used for background illumination, and the images were acquired using a high-resolution CCD camera (Pulnix TM-1040) controlled by a computer frame grabber system (Streams 5, IO Industries Inc.) with a frame rate of 30 fps and an exposure time of 1/4000 s.

A double-tip optical fiber probe system (RBI Instrumentation) based on the phase-detection technique was used to measure bubble properties. This system consists of a module that emits infrared light through two fiber-optic cables to the tips of the

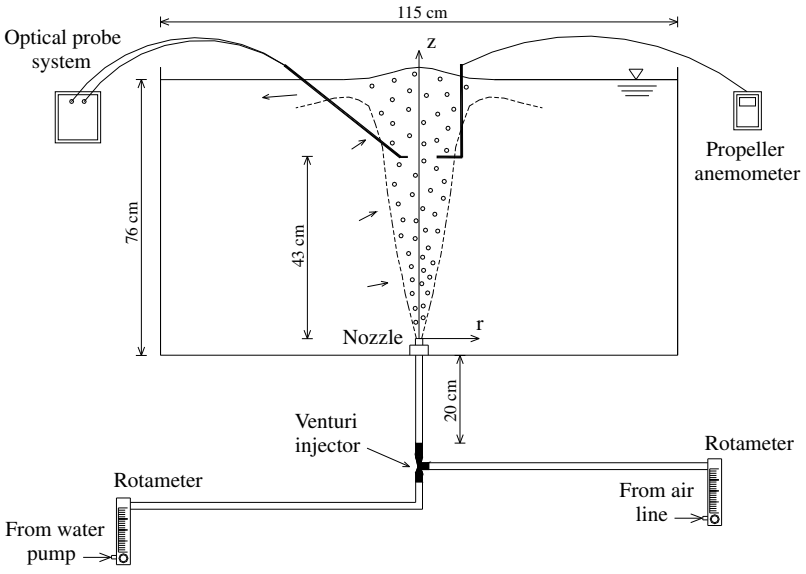

Fig. 1. Schematic of experimental apparatus.

Table 1
Summary of experimental conditions, including bubbly jets and pure water jets

Experiments	d_o (mm)	Q_{ao} (l/min)	Q_{wo} (l/min)	C_o (%)	U_{wo} (cm/s)	Re
a-0.4-5	6	0.4	5	7.4	295	17,684
a-1-5	6	1	5	16.7	295	17,684
a-2-5	6	2	5	28.6	295	17,684
a-3-5	6	3	5	37.5	295	17,684
a-4-5	6	4	5	44.4	295	17,684
a-5-1	6	5	1	83.3	59	3537
a-5-2	6	5	2	71.4	118	7074
a-5-3	6	5	3	62.5	177	10,610
a-5-4	6	5	4	55.6	236	14,147
a-1-1	6	1	1	50.0	59	3537
a-3-3	6	3	3	50.0	177	10,610
a-5-5	6	5	5	50.0	295	17,684
b-1-1	4	1	1	50.0	133	5305
b-1-2	4	1	2	33.3	265	10,610
b-5-2	4	5	2	71.4	265	10,610
c-0.4-7	9	0.4	7	5.4	183	16,505
c-2-2	9	2	2	50.0	52	4716
c-2-5	9	2	5	28.6	131	11,789
c-5-3	9	5	3	62.5	79	7074
d-3-3	13.5	3	3	50.0	35	4716
d-3-7	13.5	3	7	30.0	82	11,003
a-0-2	6	0	2	0.0	118	7074
a-0-3	6	0	3	0.0	177	10,610
a-0-4	6	0	4	0.0	236	14,147
a-0-5	6	0	5	0.0	295	17,684
b-0-2	4	0	2	0.0	265	10,610
c-0-5	9	0	5	0.0	131	11,789
c-0-7	9	0	7	0.0	183	16,505
d-0-7	13.5	0	7	0.0	82	11,003

The alphabet in the notation of the experiments corresponds to different nozzle diameters while the numbers correspond to the air and water flow rates, respectively. C_o and Re are defined in the text [see (1) and (2)]. Bubbly jet experiments include group 1 ($Re > 8000$) and group 2 ($Re < 8000$).

probe, 2 mm apart. Each tip extends 1.5 cm and is sharpened into a 30 μm diameter. Emitted light reflects back to the module when the tips pierce a bubble, resulting in a two-state signal which is recorded at a sampling rate of up to 1 MHz. Similar RBI double-tip optical fiber probe systems have been used to measure two-phase flow characteristics in bubbly flows (Rensen and Roig, 2001; Chaumat et al., 2005).

The signals obtained from the optical fiber probe system were processed to calculate the local void fraction or volumetric air concentration (C), bubble frequency (f_b), and absolute bubble velocity (u_b). Note that C is defined as the fraction of the total sampling time in which the tips of the probe are in contact with the air phase, which differs from the definition of C_o described by (1). The bubble volume-equivalent sphere diameter (d_b) was then estimated as following (Herringe and Davis, 1976):

$$d_b = 3Cu_b/2f_b \tag{3}$$

Although this equation has been developed assuming spherical bubbles rising rectilinearly, which did not necessarily occur in the experiments, preliminary optical probe tests conducted by the authors in disperse bubble plumes with bubble diameters ranging from about 2 to 10 mm provided an underestimation of d_b of only about 10%, as compared to that obtained from imaging (see Lima Neto, 2007). On the other hand, if we multiply the right hand-side of (3) by $\chi^{2/3}$ to account for the non-sphericity of the bubbles (see Moursali et al., 1995), where χ is their average ratio of the major and minor axes, we obtain an overestimation of d_b of up to about 30%, as compared to imaging. Eq. (3) has also been validated for bubbles with diameters ranging from about 4 to 7 mm (Chaumat et al., 2005) and is expected to be reliable for the purposes of this study.

Measuring the turbulent liquid flow field within the bubble core using particle image velocimetry was difficult since our flows had relatively high void fractions (i.e., up to about 4 times those of Risso and Ellingsen, 2002). Alternatively, visualization of the entrained liquid jet was achieved using laser-induced fluorescence (LIF). A similar LIF system has been used by Socolofsky (2001) for visualization of the entrained flow induced by bubble plumes. Measurements of the mean vertical water velocity inside the bubble core were performed with an electromagnetic propeller anemometer (Omni Instruments, MiniWater20) with an internal diameter of 22 mm. This anemometer is suitable for velocities higher than 2 cm/s, with an accuracy of 2% when used in pure water, and similar propeller anemometers have been used to measure the mean vertical water velocity in bubble plumes (Milgram, 1983; Fanneløp et al., 1991). The measurement error due to air bubbles in the water is deemed negligible for void fractions lower than 4%, as is the case in this study. The reliability of our propeller anemometer for measurements in vertical bubbly flows with void fractions of up to 3.5% was also confirmed by Lima Neto (2007).

Both optical probe and anemometer measurements were taken at radial distances (r) of 0, 2, 4 and 6 cm from the bubbly jet centerline and at a height (z) of 43 cm above the nozzle exit. The experiments were carried out for duration of 2 min, which was enough time to obtain stable measurements. The increase in water level due to water injection in the tank was less than 1% over the duration of each experiment, and this effect was considered negligible.

3. Results and discussion

3.1. Bubble properties and flow structure

Visual observations of the rising bubbles showed that their size did not change significantly with distance from the nozzle, as observed by Risso and Ellingsen (2002) for a disperse bubble column with a water depth of 0.70 m. Bubbles of relatively uniform sizes were generated in our tests, with the exception of experiments a-1-1, a-5-1, a-5-2, b-1-1, c-2-2, c-5-3 and d-3-3 (see Fig. 2), where

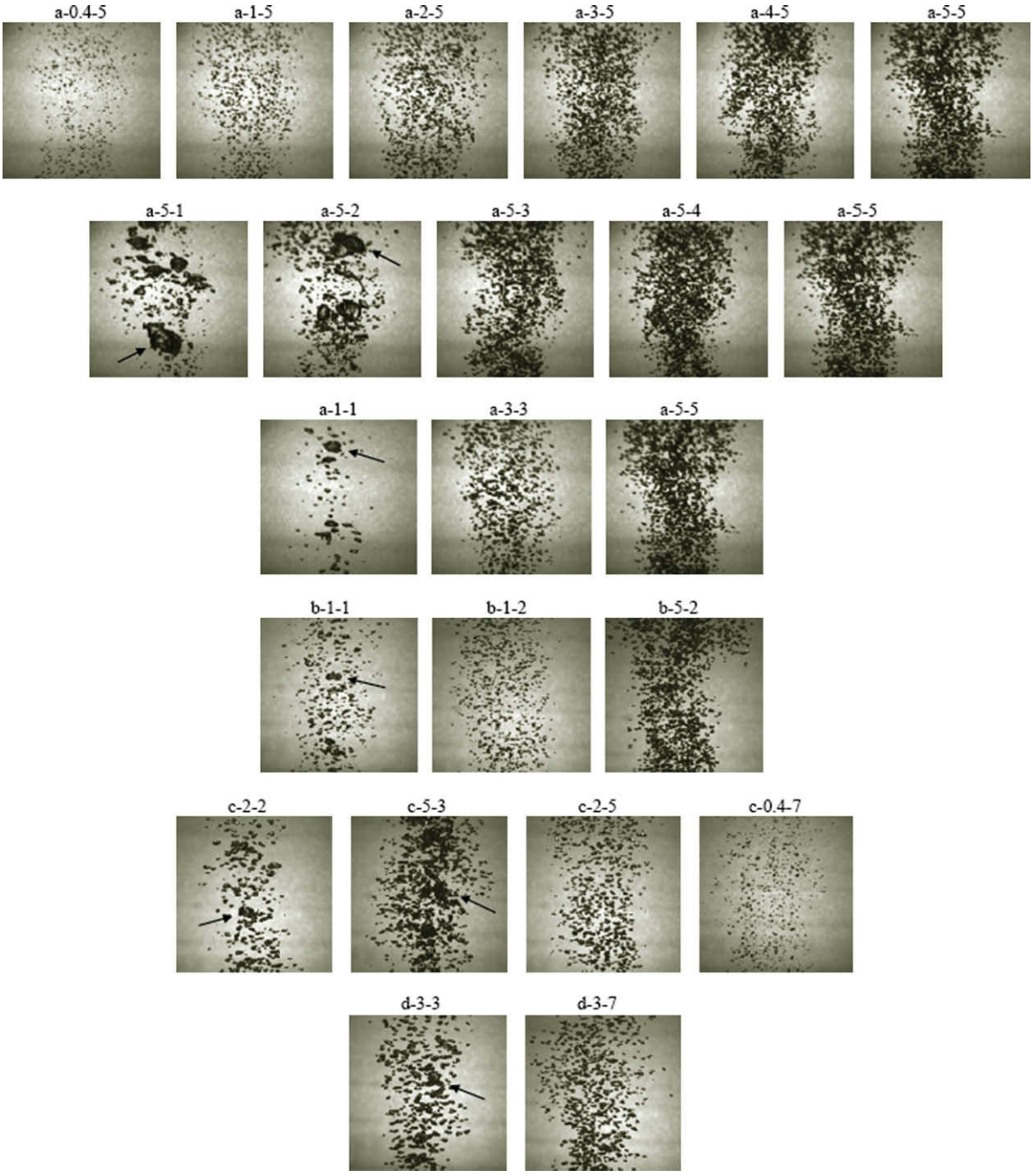

Fig. 2. Bubble images for each experiment (images of 15 × 15 cm^2 with their centers at r = 0 and z = 43 cm). Arrows indicate bubbles with volume-equivalent sphere diameter larger than 8 mm.

large and irregular bubbles were also observed. Note that the alphabet in the experiment notation (e.g. a-1-1) indicates the different types of the nozzle, while the first and second numbers give the air flow rate and water flow rate in liters per minute, respectively. Fig. 2 clearly shows that the increase of the water flow rate generates more uniform bubble sizes. In this paper, we will refer to the experiments with relatively uniform bubble sizes as group 1 and to those with large and irregular bubbles as group 2 (see Table 1).

The time series of bubble properties indicated a low-frequency periodic fluctuation about the mean value, which corresponded to a lateral oscillation of the bubble core of less than about ±3°, with a frequency ranging from about 0.02 to 0.06 Hz. The occurrence of such oscillations, also called wandering motions, is usually attributed to buoyancy driven-instabilities and the effect of the tank walls (see Rensen and Roig, 2001; Lima Neto et al., 2008). Fig. 3 shows a typical variation of the 'instantaneous' void fraction (averaged over 2 s) measured with the two fiber-optic sensors of the RBI probe, in which the global averaged (over 2 min) value of C was about 1.6% and the frequency of oscillation was about 0.05 Hz. The difference between the average void fraction measured by the first and second sensors was less than 5%, which suggests that the number of bubbles missed by the sensors due to non-rectilinear motion was not significant. It is important to mention that

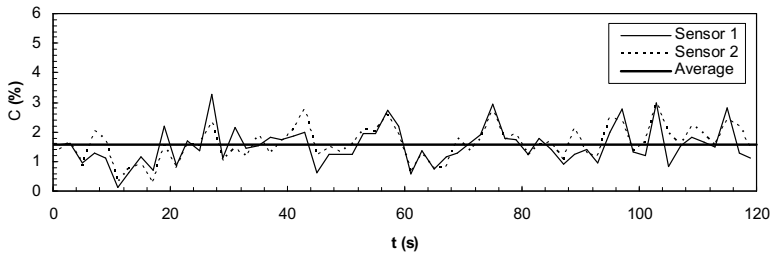

Fig. 3. Typical void fraction time series (experiment a-3-3). Note that the 'instantaneous' void fraction was averaged over 2 s. Measurements taken at $r = 0$ cm and $z = 43$ cm.

swirl motion was also present during a short period of time for some tests (especially for higher air flow rates and lower water flow rates), but the measurements were taken avoiding such conditions. On the other hand, audible cavitation (see Gavigan et al., 1974) has not been observed during the tests. Such condition was observed, however, when pure air was injected at flow rates higher than 5 L/min through single orifice nozzles of smaller diameters (<3 mm).

Fig. 4 shows typical bubble size distributions obtained from optical probe measurements at the jet centerline, all resembling lognormal curves. However, for the experiments in group 1, the range of bubble sizes is smaller (narrower band) than that for experiments in group 2, which confirms that more uniform bubbles are generated in the former case, as discussed above (see Fig. 2). It can also be seen that the peaks of the distributions increase along with the gas volume fraction with the result that more bubbles are generated (e.g., see curves for experiments a-1-5 and a-3-5), and are displaced to the left as the nozzle Reynolds number increases such that the bubble diameter decreases (e.g., see curves for experiments a-3-3 and a-3-5).

Typical radial distributions of time-averaged void fraction (C), bubble frequency (f_b), absolute bubble velocity (u_b), and bubble volume-equivalent sphere diameter (d_b) for each experiment are shown in Fig. 5. Gaussian distributions were shown to conform well to all experimental data other than the bubble diameter, which decreased by about 10% from $r = 0$ to 6 cm for the experiments in group 1. Line types indicate fitted curves to the data with the same nozzle Reynolds numbers. Assuming axisymmetry of void fraction and bubble velocity profiles, the volumetric flow rate of air at $z = 43$ cm can be calculated as follows:

$$Q_a = 2\pi \int_0^\infty C(r) u_b(r) r \, dr \tag{4}$$

Although void fraction profiles for the experiments in group 1 did not behave similarly to those in group 2 [see Fig. 5(a)], the use of Eq. (4) with the measured values of C and u_b resulted in volumetric flow rates of air within 17% of those obtained at the nozzle exit (Q_{ao}). This gives credence to our measurements as reductions in the gas flow rate with height are expected to be negligible under the present shallow water conditions. Bubble

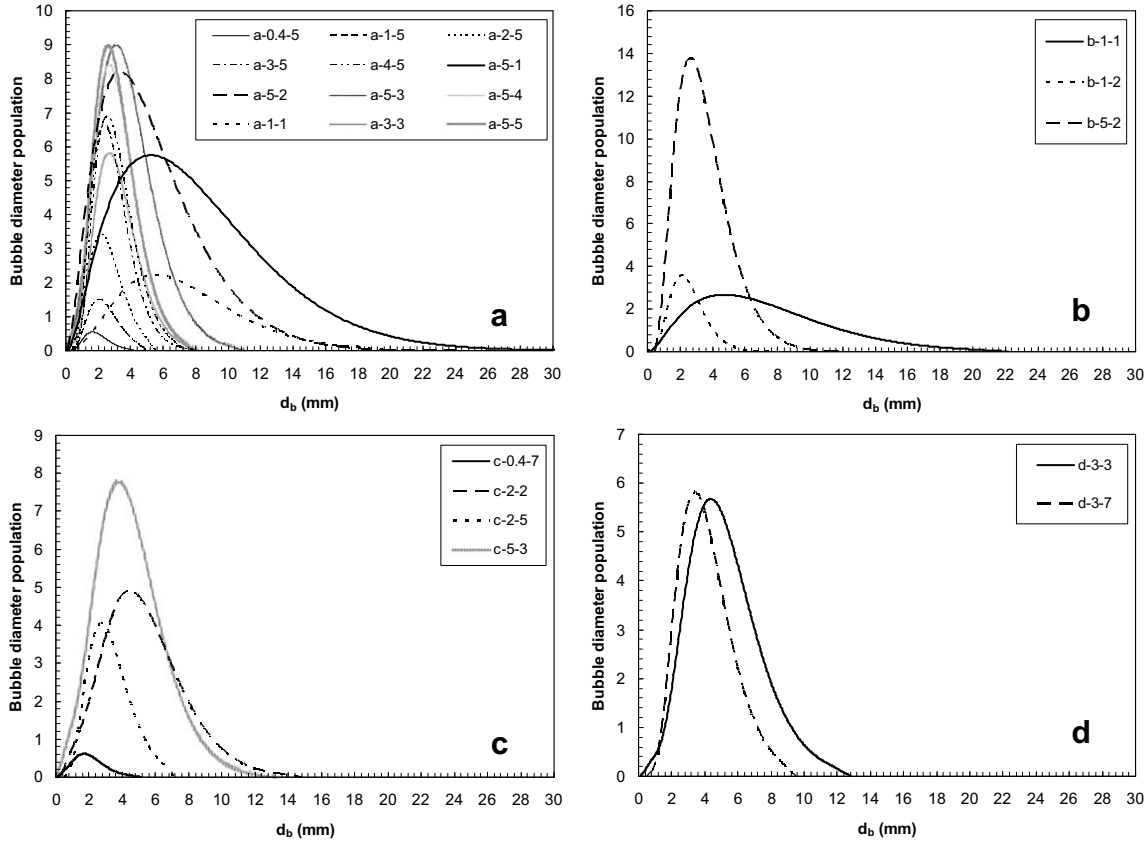

Fig. 4. Bubble size distributions obtained from optical probe measurements at $r = 0$ cm and $z = 43$ cm.

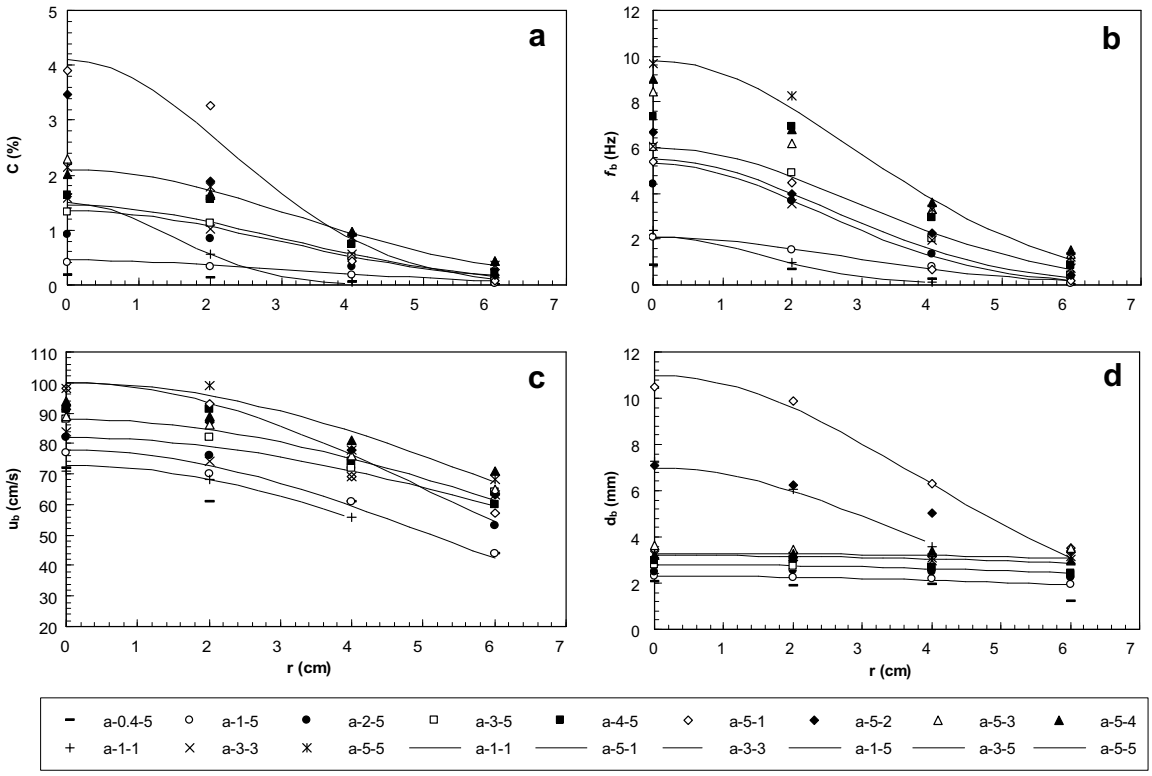

Fig. 5. Typical time-averaged radial distributions of: (a) void fraction, (b) bubble frequency, (c) absolute bubble velocity, and (d) bubble diameter for each experimental condition. Measurements were taken at $z = 43$ cm. Line types indicate fitted curves to the experimental data.

frequency and diameter profiles also behaved differently for the two groups of experiments, whereas bubble velocities did not vary significantly [see Fig. 5(b)–(d)]. For instance, bubble frequency and diameter for experiments a-5-1 and a-5-5 presented a twofold difference even though bubble velocity was of the same order. Similar behaviors can also be observed for experiments a-1-1 and a-1-5, for example. Bubble diameters shown in Fig. 5(d) ranged from 1.2 to 10.5 mm and were about 10% smaller than those obtained from the CCD camera images shown in Fig. 2, while bubble velocities shown in Fig. 5(c) ranged from 44 to 98 cm/s and were about 25% larger than those obtained from the images. Note that, for the experiments with dense bubble clouds, this comparison was only possible closer to the border of the bubble core, where individual bubbles could be better visualized.

The effect of the gas volume fraction at the nozzle (C_o) on bubble characteristics (shown in Fig. 5) was relatively strong. For experiments a-3-5 and a-5-5, for example, we can see from the corresponding fitted Gaussian curves that an increase in C_o of 33% resulted in increases in C, f_b, u_b, and d_b of approximately 70%, 60%, 10%, and 20%, respectively. Conversely, the impact of the nozzle Reynolds number in these experiments was relatively weak. An increase in Re of 67% resulted in decreases in C and d_b by only 10% and increases in f_b and u_b by only about 20% and 10%, respectively.

The centerline values of time-averaged absolute bubble velocity (u_{bc}) and bubble volume-equivalent sphere diameter (d_{bc}) are non-dimensionalized by velocity and length scales defined, respectively, by $U = Q_{wo}/L^2$ and $L = (Q_{wo}^2/g)^{1/5}$, and correlate to C_o and Re in Fig. 6. The results for all experiments in group 1 collapsed to the same linear curves, indicating that the effects of C_o and Re can be appropriately incorporated into the following relationships:

$$\frac{u_{bc}}{U} = 1.678(C_o) + 1.688 \qquad (R^2 = 0.935) \tag{5}$$

$$\frac{d_{bc}}{L} = 0.341 \times 10^4 \left(\frac{C_o}{Re}\right) + 0.118 \qquad (R^2 = 0.963) \tag{6}$$

Note that Eqs. (5) and (6) are obtained at a specific height of $z = 43$ cm above the nozzle exit. The symbol R^2 stands for the coefficient of determination, which is defined as the square of the correlation between the fitted curves and experimental data.

Fig. 7 shows typical radial distributions of the axial water velocity (u_w) measured with the Omni anemometer for the experiments with and without air injection into the water jets. The values obtained for the pure water jets followed Gaussian curves in accordance with the theory of single-phase jets (see Rajaratnam, 1976). The values obtained for bubbly jets could also be fitted by Gaussian curves, with the magnitude of the velocity evidently increasing with the presence of the bubbles, as compared to pure water jets with the same Re-value. The observed axial water velocities for experiments a-5-2, a-5-3, a-5-4 and a-5-5 (with C_o ranging from 71.4% to 50.0%), for example, were about 4–2 times larger than the corresponding values for experiments a-0-2, a-0-3, a-0-4 and a-0-5 (all with $C_o = 0$), respectively (see the upper and lower Gaussian curves shown in Fig. 7). This result differs from previous measurements in confined bubbly jets, where the effect of the gas volume fraction on the mean axial liquid velocity was relatively weak. Kumar et al. (1989) and Iguchi et al. (1997) investigated confined bubbly jets in small-scale vessels for C_o-values of up to 20% and 50%, and detected increases in the axial water velocity due to the presence of the bubbles of only about 10% and 20%, respectively. However, the increase in the intensity of turbulence due to the presence of the bubbles approached 100%. This probably occurred because of the relatively small size of their set-ups limiting the entrainment rate, and resulting in a weak increase of this entrainment rate with the gas volume

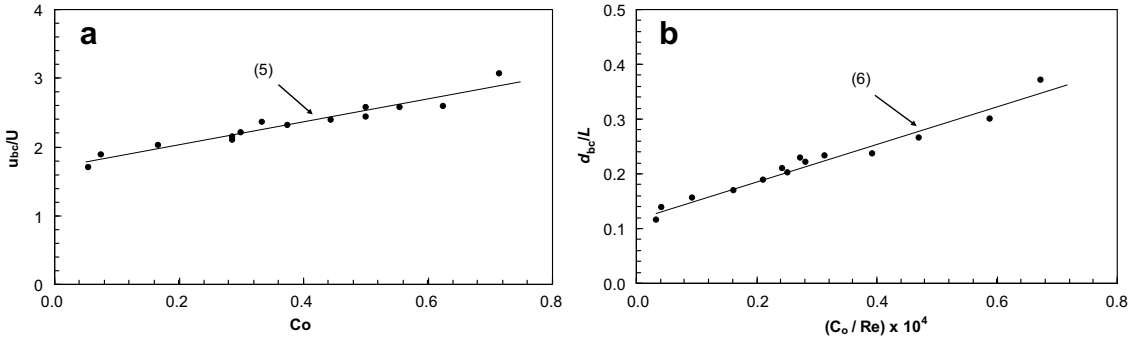

Fig. 6. Centerline values of (a) absolute bubble velocity and (b) bubble diameter. Data points include all experiments with $Re > 8000$.

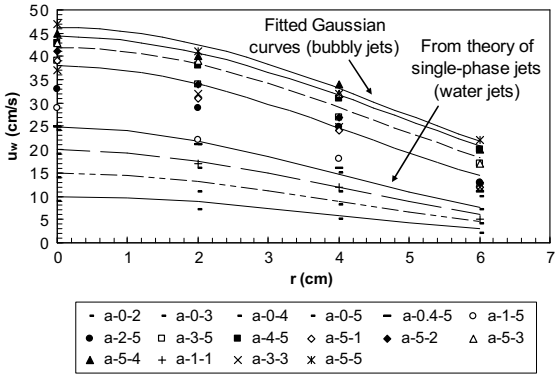

Fig. 7. Typical radial distributions of axial water velocity. Measurements were taken at $z = 43$ cm. Lower and upper lines indicate fitted curves for pure water jets (a-0-2, a-0-3, a-0-4 and a-0-5) and bubbly jets (a-5-2, a-5-3, a-5-4 and a-5-5), respectively.

fraction. In our case, the effect of the nozzle Reynolds number on measurements of axial water velocity was relatively weak. For experiments a-5-3 and a-5-5 (or a-3-3 and a-3-5), for example, an increase in *Re*-value of 67% resulted in an increase in u_w of only about 10% (observe the upper Gaussian curves in Fig. 7). The following dimensionless relationship was rendered by the curve-fitting of experimental data for the experiments in group 1 to describe the effect of C_o and *Re* on the axial water velocity:

$$\frac{u_{wc}}{U} = 0.013(C_o^3 Re)^{1/2} + 0.588 \qquad (R^2 = 0.972) \tag{7}$$

where u_{wc} is the axial water velocity at the centerline. Fig. 8(a) shows that (7) fitted well to the experimental data.

We also studied other dimensionless relationships to describe the behavior of the bubbly jets using similar parameters as those used for single-phase buoyant jets (see Jirka, 2004), such as a densimetric Froude number $[Fr = U_{wo}/(d_o g \Delta\rho/\rho_w)^{0.5}]$, length and velocity scales based on the kinematic fluxes of momentum ($M_o = Q_{wo}U_{wo}$) and buoyancy ($B_o = Q_{ao} g \Delta\rho/\rho_w$), where $\Delta\rho$ is the difference between the water density, ρ_w, and the air density; ρ_a, as well as other scales such as d_o and U_{wo}. However, the experimental data did not collapse well to single curves, resulting in lower correlation coefficients than those obtained by using the scales *L* and *U* and the parameters C_o and *Re*. This is consistent with the work of Iguchi et al. (1997), where the behavior of bubbly jets could be described as a function of C_o, for a fixed value of *Re*. Note that in our study, the effect of volume fluxes is also incorporated into the scales *L* and *U*, which are functions of $Q_{wo}^{2/5}$ and $Q_{wo}^{1/5}$, respectively. Therefore, we believe that the parameters C_o and *Re* are sufficient to describe the behavior of bubbly jets when using the scales *L* and *U*.

We define r_w and r_b as characteristic radii of the water jet and bubble core where $u_w = e^{-1}u_{wc}$ and $C = e^{-1}C_c$, respectively. Fitting Gaussian curves to the water velocity profiles (see Fig. 7) and neglecting the virtual origin of the jets, we find a linear spreading of the water jet radius, r_w/z, of about 0.12 for pure water jets, 0.11 for bubbly jets in group 2, and 0.14 for bubbly jets in group 1. We estimate an uncertainty in these spreading rates of about 10% due to the above assumptions. Laser-induced fluorescence (LIF) images shown in Fig. 9 confirm that the jets spread linearly. Note that the spreading obtained from LIF images (of about 0.18) corresponds to the spreading of the edge of the water jets (where $u_w = 0$), which is higher than the spreading of r_w obtained from water velocity measurements (where $u_w = e^{-1}u_{wc}$). The spreading rates of r_w obtained here are close to the value of 0.11 reported by Turner (1986) for single-phase jets and plumes, and are within the range of typical

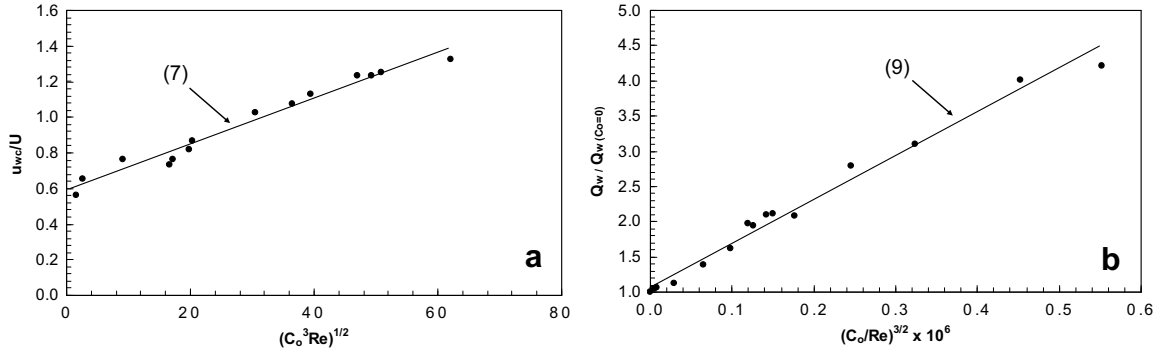

Fig. 8. (a) Centerline values of axial water velocity and (b) liquid volume flux of the bubbly jet relative to that of a pure water jet with the same nozzle diameters and water flow rates. Data points include all experiments with $Re > 8000$.

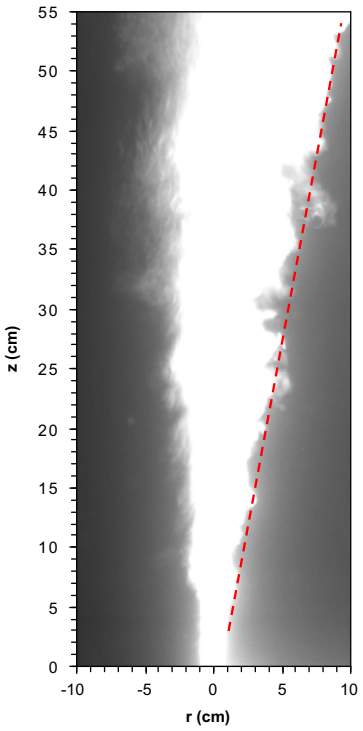

Fig. 9. Typical LIF image of the bubbly jets (experiment a-3-3). Dashed line indicates a linear spreading of the water jet with height. Note that the left-hand side of the water jet is not completely visualized because the bubbles blocked the laser sheet, which was launched from the right-hand side.

values of 0.10–0.20 reported by Milgram (1983), Socolofsky (2001) and Brevik and Kristiansen (2002) for bubble plumes. A linear spreading ratio of the bubble core radius relative to the water jet radius, r_b/r_w, of about 0.55 for bubbly jets in group 2 and 0.70 for bubbly jets in group 1 is obtained by fitting Gaussian curves to the void fraction profiles [see Fig. 5(a)]. Again, the spreading ratios obtained here are within the range of typical values of 0.50–0.90 reported by Milgram (1983), Socolofsky (2001) and Brevik and Kristiansen (2002) for bubble plumes.

With the assumption that we have a linear spreading of the water jet radius, Gaussian profiles of axial water velocity, and a constant entrainment coefficient, the liquid volume flux increases linearly with z (Rajaratnam, 1976):

$$\frac{dQ_w}{dz} = 2\pi r_w \alpha u_{wc} \tag{8}$$

where α is the entrainment coefficient. The entrainment coefficient can be obtained by solving (8) for the water flow rates at the nozzle exit, Q_{wo}, given in Table 1, and Q_w (which is the liquid volume flux obtained by integration of u_w in the radial direction using fitted Gaussian curves). These calculations generated values of $\alpha = 0.053$ for pure water jets and 0.056 for bubbly jets, which are closer to the value of 0.054 reported by Turner (1986) for single-phase jets than the value of 0.083 for single-phase plumes, and are within the typical range of values, 0.03–0.15, reported by Milgram (1983), Socolofsky (2001) and Brevik and Kristiansen (2002) for bubble plumes.

The liquid volume flux of a bubbly jet Q_w is compared to that of a pure water jet $Q_{w(C_o=0)}$ with the same nozzle diameters and water flow rates in Fig. 8(b). Here, Q_w was obtained by direct integration of the axial water velocity profiles, as given in Fig. 7. Eq. (6) was obtained by the curve fitting of experimental data for the experiments in group 1. Fig. 8(b) shows that $Q_w/Q_{w(C_o=0)}$ increases linearly with $(C_o/Re)^{3/2}$, reaching a maximum of about 4.2 for experiment b-5-2. This result indicates that the liquid volume flux can be increased by more than 300% when $C_o = 0.71$ and $Re = 10{,}610$:

$$\frac{Q_w}{Q_{w(C_o=0)}} = 1 + 6.426 \times 10^6 \left(\frac{C_o}{Re}\right)^{3/2} \qquad (R^2 = 0.980) \tag{9}$$

The increase in the liquid volume flux described by Eq. (9) can perhaps be attributed to additional entrainment into the wakes of the bubbles, which increase in velocity and size as C_o increases [see Fig. 6]. Based on the results of Uberoi and Freymuth (1970) for wakes behind a solid sphere, Leitch and Baines (1989) estimated that the entrainment associated with the bubble wakes generated by weak air injection in water ranged from 26% to 64% of the entrainment with the water jet surrounding the bubble core, with this ratio also increasing along with the gas flow rate. In the present study, it was not plausible to estimate the contribution of the wake of each bubble individually because the space between the bubbles was much smaller than the extent of the isolated wakes studied by Uberoi and Freymuth (1970). Accordingly, additional liquid turbulence caused by interactions of the bubbles and their wakes might also have contributed to the increase in liquid volume flux described by (9). This is consistent with the results of Hetsroni (1989), where particles with Reynolds numbers $Re_p > 400$ tend to enhance turbulence in the flow, as in our case (see Section 3.2), while particles with $Re_p < 400$ tend to suppress it. Similarly, Brevik and Kluge (1999), based on experimental observation of mean flow patterns in unconfined bubble plumes, assumed self-preservation of turbulent velocities fluctuations and estimated a ratio between the vertical turbulent kinetic energy and the vertical mean kinetic energy of about 30%, which is considerably higher than that obtained in single-phase free jets (about 10%). The increase of $Q_w/Q_{w(C_o=0)}$ with $(C_o/Re)^{3/2}$ is also consistent with the results of Kumar et al. (1989), where the increase in turbulence intensities was more pronounced at higher gas volume fractions and lower nozzle Reynolds numbers. In the study conducted by Iguchi et al. (1997), the turbulence intensity also increased in conjunction with the gas volume fraction, but unfortunately their study only presented measurements of turbulence at one nozzle Reynolds number, so we cannot compare with their results. A more recent study conducted by Risso and Ellingsen (2002) in a dilute bubble column also showed that, at a considerable distance from the bubbles, the liquid velocity fluctuations linked to non-linear interactions with bubble wakes scaled with the void fraction as $C^{0.4}$. However, their study was limited to gas injection with local void fractions up to about 1% and cannot be directly compared to our results.

We also compared the results of the bubbly jets with those of the single-phase water jets with the same total flow rates at the nozzle, which corresponds to the tests a-1-1 and a-0-2, b-1-1 and b-0-2, and c-2-5 and c-0-7. The values of Q_w in bubbly jets range from about 40% to 150% higher than those of the corresponding water jets with the same total flow rates. Increases in Q_w of up to about 140% were also obtained for the other experimental conditions by estimating the liquid volume flux in single-phase jets using the theory of free jets (see Rajaratnam, 1976). We also compared the liquid volume fluxes induced by our bubbly jets to those estimated using the theory of single-phase buoyant jets (see Jirka, 2004), considering the same kinematic fluxes of momentum, M_o, and buoyancy, B_o, in both cases. Similarly, increases in Q_w of up to about 180% were also obtained. Therefore, we can conclude that bubbly jets induce higher liquid volume fluxes than single-phase jets with the same total flow rates and than single-phase buoyant jets with the same kinematic fluxes of momentum and buoyancy.

This implies that bubble wakes and their interactions with the main flow play an important role on the total liquid volume flux induced by bubbly jets, as suggested by Leitch and Baines (1989) for bubble plumes.

3.2. Bubble slip velocity, shape and drag coefficient

Fig. 10(a) shows bubble slip velocities (u_s) obtained by subtracting the water velocities induced by the bubbly jets from the absolute bubble velocities. Data obtained from Lima Neto (2007) by means of experiments on bubble plumes generated through different nozzle types is also presented in this figure. It can be seen that, for both bubbly jets and bubble plumes, bubble slip velocity can be described as a function of bubble volume-equivalent sphere diameter, d_b. This suggests that the effect of void fraction (in our case, up to about 4%) on the bubble slip velocity was relatively small. The values of u_s obtained here follow similar trends but are higher than the terminal bubble velocities given by Clift et al. (1978) for isolated bubbles with diameters ranging from about 1 to 10 mm. This occurrence can be attributed to the fact that trailing bubbles in the wake of leading bubbles rise faster than isolated bubbles due to drag reduction, as observed by Ruzicka (2000) with experiments on bubbles rising in line. The maximum bubble slip velocity obtained in the present study was 70 cm/s, which is consistent with the values of up to about 80 cm/s obtained by Simonnet et al. (2007) in a bubble column with similar bubble diameters as those generated here, but with void fraction of about 9 times higher (i.e., up to 35%). The above slip velocities are approximately 2 times higher than the rising velocity of isolated bubbles with the same diameters. This significant increase in the slip velocity is also consistent with the results obtained by Krishna et al. (1999) in bubble columns with void fractions ranging from about 5% to 25%, where the rising velocity of large bubble swarms was found to be 3 to 6 times higher than that of isolated bubbles. The results obtained from Sankaranarayanan et al. (2002) by numerical simulations of the flow in bubbly suspensions with large bubbles also confirmed this increase in the bubble swarm velocity as compared to that of isolated bubbles.

Using the bubble diameters and slip velocities estimated above, we can calculate the bubble Reynolds number ($Re_b = u_s d_b/\nu_w$), Eötvös number ($E_b = g\Delta\rho d_b^2/\sigma$), and Morton number ($M_b = g\Delta\rho\mu_w^4/\rho_w^2\sigma^3$), where σ is the air–water surface tension and μ_w is the viscosity of water. These dimensionless numbers are generally used to express the importance of inertia, buoyancy, surface tension, and viscosity on single bubbles rising in liquids. For the present experiments, the ranges of Re_b and E_b were 406–8627 and 0.2–19.5, respectively, and $M_b = 3.1 \times 10^{-11}$. According to the classical diagram describing the behavior of isolated bubbles provided by Clift et al. (1978), our values of Re_b, E_b and M_b fall within the region of spherical, ellipsoidal and wobbling regimes, which is in agreement with the shapes observed from the CCD images (see Fig. 2).

As mentioned above, changes in the size of the rising bubbles were negligibly small under the present experimental conditions. Thus, assuming that the bubble slip velocity is only a function of bubble diameter and does not vary with axial distance from the nozzle, the drag coefficient can be estimated by equating the drag force imposed by the bubbles to their buoyancy, as shown in the following equation:

$$C_D = \frac{4 d_b g \Delta\rho}{3 \rho_w u_s^2} \tag{10}$$

Experimental results obtained by Felton and Loth (2001) for spherical bubbles with diameters of 0.4–1.2 mm moving in a turbulent boundary layer with free stream velocities between 0.40 and 0.90 m/s support the approximation given by (10). In their study, drag and buoyancy forces were of the same magnitude while the other terms involved in the force balance (i.e., liquid stress gradient resulting from fluid acceleration and lift force arising from nonzero vorticity in the liquid flow), accounted for only 10% and 25% of those, respectively. In our case, we anticipate an even higher contribution of the buoyancy forces since the bubble diameters are larger, ranging from 1 to 10 mm, and a smaller contribution of the liquid stress gradient and lift force since our centerline water velocities are smaller, ranging from 0.23 to 0.47 m/s. An experimental study conducted by Ford and Loth (1998) on ellipsoidal bubbles moving in a turbulent shear layer with liquid velocities between 0.20 and 0.43 m/s also exhibited lift forces close to zero for bubbles with diameters ranging from 1.5 to 3.5 mm, and even negative values for bubbles with a 4.5 mm diameter. With these caveats, we expect our approximation of drag being balanced by buoyancy to be reasonable.

The variation of C_D [calculated using (10)] with Re_b is shown in Fig. 10(b). It is observed that the drag coefficient can be described as a function of the bubble Reynolds number. The values of C_D obtained here follow similar trends but are smaller than those given by Clift et al. (1978) for isolated bubbles with Re_b ranging from about 700 to 9000. As mentioned, this must have occurred as a result of the fact that trailing bubbles in the wake of leading bubbles experience drag reduction (see Ruzicka, 2000). Moreover, in the curve obtained by Clift et al. (1978), we find a minimum at about $Re_b = 400$ corresponding to the onset of bubble oscillations, where the small bubbles enter the ellipsoidal regime and the drag coefficient can be seen to increase significantly with Re_b until it reaches the spherical-cap regime and becomes approximately constant. Our results, however, show a delay in this minimum, which

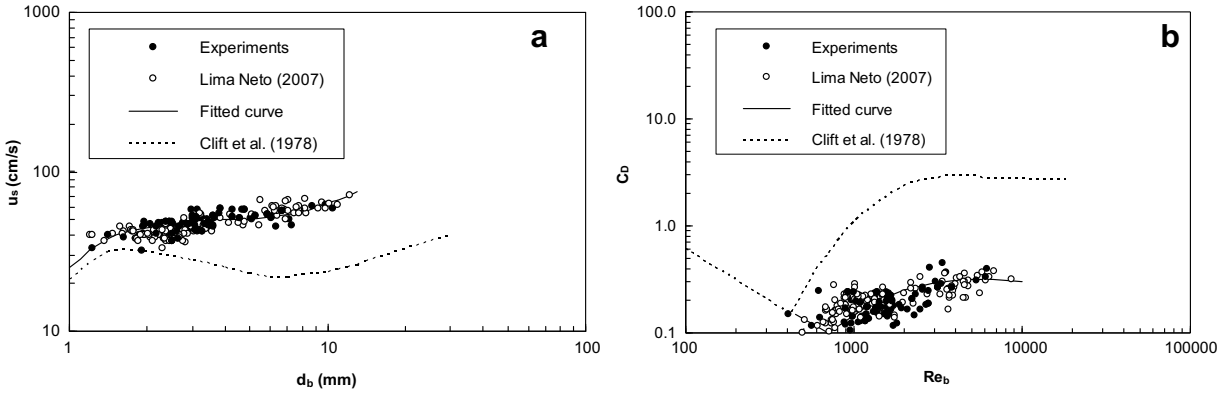

Fig. 10. (a) Variation of bubble slip velocity with bubble diameter and (b) variation of drag coefficient [calculated using (10)] with bubble Reynolds number.

appears to occur at about $Re_b = 700$. Additionally, the increase in C_D beyond this point is much more gradual than that for isolated bubbles.

3.3. Bubble breakup

For bubbly jets, we expect bubble breakup to occur both at the nozzle and in the bubbly jet region. Because of the high void fraction close to the nozzle exit, we were not able to visualize individual bubbles up to a height of about $z = 15d_o$ (i.e., from 6 to 20 cm), where bubble breakup processes are expected to be complete (see Sevik and Park, 1973). However, as mentioned above, we were able to observe the bubbles from $z = 35.5$ to 50.5 cm (see Fig. 2), where the experiments in group 2 presented a wider range of bubble sizes than that in group 1 (see Fig. 4). Group 2 corresponded to the experiments with lower nozzle Reynolds numbers (i.e., $Re < 7100$) (see Table 1), which suggests that for such conditions, turbulence was not fully developed and the eddies were not strong enough to cause breakup of the larger bubbles at the nozzle or above it. The other group of experiments (group 1) with smaller and more uniform bubbles correspond to nozzle Reynolds numbers exceeding 10,600. We can thus conclude that a transition Reynolds number lies between these two values. Fig. 11(a) and (b) shows, respectively, the effect of Re on the time-averaged bubble volume-equivalent sphere diameter (d_{bc}) and on the maximum bubble diameter ($d_{b,max}$), estimated here by taking the bubble diameter corresponding to 90% of the area under the curves shown in Fig. 4. In those figures, it is clearly seen that for the tests with $Re < 8000$, the values of d_{bc} and $d_{b,max}$ are larger than 4 and 8 mm, respectively. Therefore, we propose that a minimum nozzle Reynolds number of 8000 is needed to produce sufficiently strong turbulence to generate more uniform and smaller bubbles due to breakup close to the nozzle.

Our proposed critical Reynolds number at the nozzle is consistent with the results of Sun and Faeth (1986a,b) and Iguchi et al. (1997), in which bubbles with approximately uniform diameters of about 1–2 mm were observed photographically for experiments with Re-values exceeding about 8200 and 10,700, respectively. It should be noted that both of these studies omitted experiments involving lower nozzle Reynolds numbers. Interestingly, bubbles with approximately uniform sizes were observed photographically by Kumar et al. (1989) at a smaller nozzle Reynolds number of $Re = 4700$. However, that study used a screen assembly to breakup large bubbles and to produce a more uniform mixture. Therefore, we expect that a minimum value of $Re = 8000$ is necessary to produce bubbles of approximately uniform sizes, independent of the gas volume fraction.

Although bubble breakup processes in most tests conducted here were complete at $z = 35.5$ cm, we still observed breakup from $z = 35.5$ to 50.5 cm (see Fig. 2) of a few large bubbles in experiments a-5-1 and a-5-2. In this case, we could analyze bubble breakup more precisely by considering the local Weber number. This dimensionless number relates inertial forces and surface tension forces and is believed to be the controlling parameter for bubble breakup in turbulent flow. The Weber number is usually defined based on a length scale, taken as the volume-equivalent sphere diameter of the bubbles, and mean or turbulent velocity scales (see Hinze, 1955; Clift et al., 1978). However, as pointed out by Risso and Fabre (1998), the theory for bubble breakup is still incomplete and the correct breakup criterion should take into account not only the mean velocity components but also the turbulence level and residence time of the bubbles in the flow, which

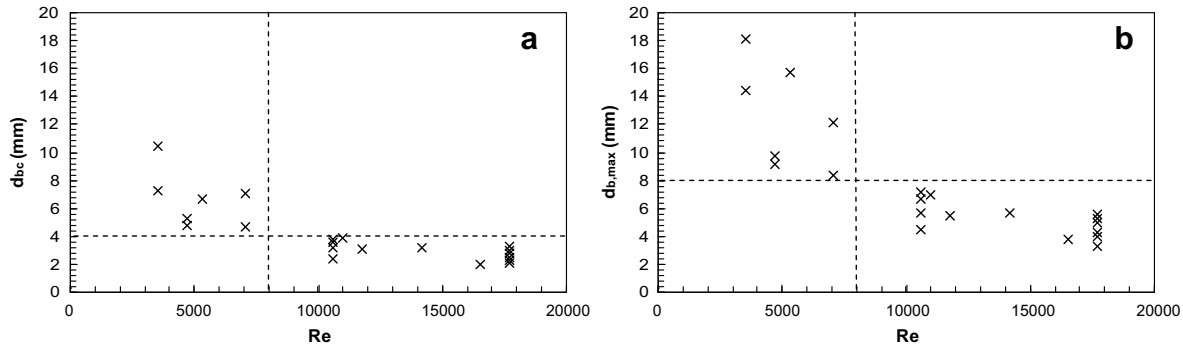

Fig. 11. Effect of nozzle Reynolds number on the (a) time-averaged bubble volume-equivalent sphere diameter and (b) maximum bubble diameter.

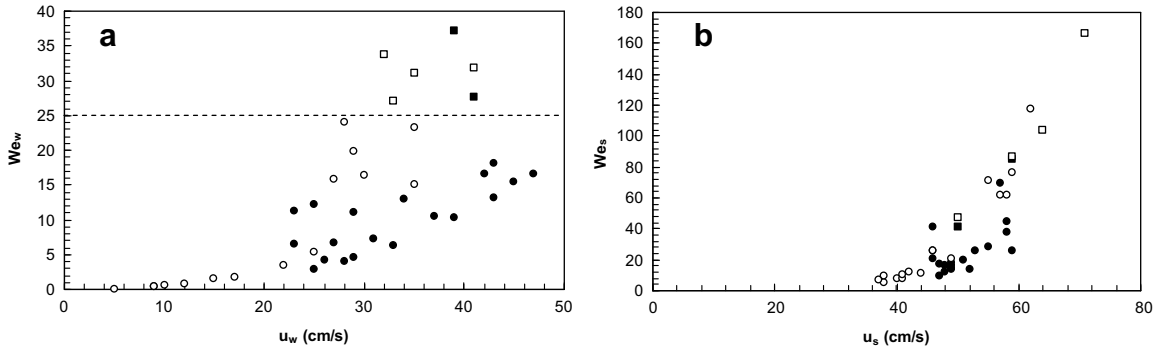

Fig. 12. (a) Weber numbers based on mean water velocity, indicating a limit of $We_w = 25$ above which bubble breakup occurs, and (b) Weber numbers based on bubble slip velocity. Bubbly jet tests with and without breakup are represented, respectively, by the symbols ■ and ●, while bubble plume tests (from Lima Neto, 2007) with and without breakup are represented, respectively, by the symbols □ and ○.

are not well understood even in the simple case of isolated bubbles in water. Therefore, in the absence of detailed information on the more complex flows in the present study, we will use the following definitions for the Weber number based on the mean water velocity (u_w) and the bubble slip velocity (u_s):

$$We_w = \rho u_w^2 d_{b,max}/\sigma \quad (11)$$

$$We_s = \rho u_s^2 d_{b,max}/\sigma \quad (12)$$

Fig. 12 shows the ranges of Weber numbers obtained by combining optical probe and anemometer measurements from this study with those from Lima Neto (2007) and using (11) and (12). In Fig. 12(a), the values of We_w varied from about 0.1 to 37 and all the experiments with occurrence of bubble breakup presented $We_w > 25$, which suggests that the deformation caused by mean water velocity significantly contributed to the breakup, while turbulence played a secondary role. This was also observed by Risso and Fabre (1998), who analyzed the data of Sevik and Park (1973) and Senhaji (1993) from experiments on single bubbles in uniform turbulent downflow and turbulent upward jet, respectively, and concluded that the role of the turbulence was to provide the small amount of energy lacking to obtain the breakup of a pre-deformed bubble. On the other hand, in Fig. 12(b), the values of We_s varied from about 5 to 166 but no consistent criteria to represent the onset of bubble breakup was obtained. Therefore, we propose that a minimum value of $We_w = 25$ is needed to produce sufficiently strong deformation of the bubbles to cause their breakup away from the nozzle in bubbly jets and bubble plumes.

4. Conclusions

An experimental study on air–water bubbly jets in a relatively large water tank was carried out to investigate bubble properties and mean liquid flow structure. The tests included bubbly jets with gas volume fractions, C_o, ranging from 5% to 83% and nozzle Reynolds numbers, Re, ranging from 3500 to 17,700, which produced bubbles with diameters ranging from about 1 to 10 mm. The experiments were classified into two groups, one with relatively uniform bubble sizes and another with large and irregular bubbles. For the first group, bubble properties and mean liquid flow structure could be described by dimensionless relationships as functions of C_o and Re. Injection of air into a liquid jet can significantly increase the liquid volume flux, and the rate of the increase was found to be a linear function of $(C_o Re)^{3/2}$. This increase was attributed to additional entrainment into the wakes of the bubbles and turbulence caused by interactions of the bubbles and their wakes, as reported in the literature for disperse vertical bubbly flows. Bubble slip velocities were higher than the terminal velocities for isolated bubbles, while drag coefficients were smaller. It was concluded that this trend must be tied to the fact that trailing bubbles in the wake of leading bubbles have a lower drag, allowing them to rise faster than isolated bubbles. New relationships are proposed to describe bubble slip velocity as a function of bubble diameter and drag coefficient as a function of bubble Reynolds number. These interactions are important because two-phase models for vertical bubbly flows typically assume bubble slip velocity and drag coefficient values of the same order as those for isolated bubbles.

Bubble breakup processes were also investigated in this study. It was found that for bubbly jets, a nozzle Reynolds number exceeding about $Re = 8000$ was required to breakup larger bubbles into smaller bubbles and to produce a more uniform bubble size distribution. Finally, a minimum Weber number based on the mean water velocity of $We_w = 25$ was found to be necessary to produce strong bubble deformation and breakup away from the nozzles, while the Weber number based on the slip velocity, We_s, did not provide a consistent criteria to represent the onset of breakup.

Acknowledgements

The first author is supported by the Coordination for the Improvement of Higher Education Personnel Foundation (CAPES), Ministry of Education, Brazil. The authors are thankful to Perry Fedun and Chris Krath for building the experimental apparatus.

References

Brevik, I., Kluge, R., 1999. On the role of turbulence in the phenomenological theory of plane and axisymmetric air-bubble plumes. Int. J. Multiphase Flow 25, 87–108.
Brevik, I., Kristiansen, Ø., 2002. The flow in and around air bubble plumes. Int. J. Multiphase Flow 28, 617–634.
Buscaglia, G.C., Bombardelli, F., García, M.H.A., 2002. Numerical modelling of large-scale bubble plumes accounting for mass transfer effects. Int. J. Multiphase Flow 28, 1763–1785.
Chaumat, H., Billet-Duquenne, A.M., Augier, F., Mathieu, C., Delmas, H., 2005. Application of the double optic probe technique to distorted tumbling bubbles in aqueous or organic liquid. Chem. Eng. Sci. 60, 6134–6145.
Clift, R., Grace, J.R., Weber, M.E., 1978. Bubbles, Drops and Particles. Academic Press, New York.
Fanneløp, T.K., Hirschberg, S., Küffer, J., 1991. Surface current and recirculating cells generated by bubble curtains and jets. J. Fluid Mech. 229, 629–657.
Felton, K., Loth, E., 2001. Spherical bubble motion in a turbulent boundary layer. Phys. Fluids 13, 2564–2577.
Ford, B., Loth, E., 1998. Forces on ellipsoidal bubbles in a turbulent shear layer. Phys. Fluids 10, 178–188.
Gavigan, J.J., Watson, E.E., King III, W.F., 1974. Noise generation by gas jets in a turbulent wake. J. Acoust. Soc. Am. 56, 1094–1099.
Herringe, R.A., Davis, M.R., 1976. Structural development of gas–liquid mixture flows. J. Fluid Mech. 73, 97–123.
Hetsroni, G., 1989. Particle–turbulence interaction. Int. J. Multiphase Flow 15, 735–746.
Hinze, J.O., 1955. Fundamentals of the hydrodynamic mechanism of splitting in dispersion processes. AIChE J. 1, 289–295.
Iguchi, M., Okita, K., Nakatani, T., Kasai, N., 1997. Structure of turbulent round bubbling jet generated by premixed gas and liquid injection. Int. J. Multiphase Flow 23, 249–262.
Jirka, G.H., 2004. Integral model for turbulent buoyant jets in unbounded stratified flows. Part I. Single round jet. Environ. Fluid Mech. 4, 1–56.
Krishna, R., Urseanu, M.I., Baten, J.M., Ellenberger, J., 1999. Rise velocity of a swarm of large gas bubbles in liquids. Chem. Eng. Sci. 54, 171–183.
Kumar, S., Nikitopoulos, D.N., Michaelides, E.E., 1989. Effect of bubbles on the turbulence near the exit of a liquid jet. Exp. Fluids 7, 487–494.
Leitch, A.M., Baines, W.D., 1989. Liquid volume flux in a weak bubble plume. J. Fluid Mech. 205, 77–98.
Lima Neto, I.E., 2007. Gas injection in water for artificial aeration and circulation, Ph.D. Thesis, University of Alberta, 137p.
Lima Neto, I.E., Zhu, D.Z., Rajaratnam, N., Yu, T., Spafford, M., McEachern, P., 2007. Dissolved oxygen downstream of an effluent outfall in an ice-covered river: natural and artificial aeration. J. Environ. Eng. ASCE 133, 1051–1060.
Lima Neto, I.E., Zhu, D.Z., Rajaratnam, N., 2008. Effect of tank size and geometry on the flow induced by circular bubble plumes and water jets. J. Hydraul. Eng. ASCE 134, 833–842.
Milgram, H., 1983. Mean flow in round bubble plumes. J. Fluid Mech. 133, 345–376.
Morchain, J., Moranges, C., Fonade, C., 2000. CFD modelling of a two-phase jet aerator under influence of a crossflow. Water Res. 34, 3460–3472.
Moursali, E., Marié, J.L., Bataille, J., 1995. An upward turbulent bubbly boundary layer along a vertical flat plate. Int. J. Multiphase Flow 21, 107–117.
Oddie, G., Pearson, J.R.A., 2004. Flow-rate measurement in two-phase flow. Annu. Rev. Fluid Mech. 36, 149–172.
Rajaratnam, N., 1976. Turbulent Jets. Elsevier Scientific, Amsterdam, The Netherlands.
Rensen, J., Roig, V., 2001. Experimental study of the unsteady structure of a confined bubble plume. Int. J. Multiphase Flow 27, 1431–1449.
Rensen, J., Luther, S., Lohse, D., 2005. The effect of bubbles on developed turbulence. J. Fluid Mech. 538, 153–187.
Risso, F., Ellingsen, K., 2002. Velocity fluctuations in a homogeneous dilute dispersion of high-Reynolds-number rising bubbles. J. Fluid Mech. 453, 395–410.
Risso, F., Fabre, J., 1998. Oscillations and breakup of a bubble immersed in a turbulent field. J. Fluid Mech. 372, 323–355.
Rosso, D., Stenstrom, M.K., 2006. Surfactant effects on alpha factors in aeration systems. Water Res. 40, 1397–1404.

Ruzicka, M.C., 2000. On bubbles rising in line. Int. J. Multiphase Flow 26, 1141–1181.
Sahoo, G.B., Luketina, D., 2003. Modelling of bubble plume design and oxygen transfer for reservoir restoration. Water Res. 37, 393–401.
Sankaranarayanan, K., Shan, X., Kevrekidis, I.G., Sundaresan, S., 2002. Analysis of drag and virtual mass forces in bubbly suspensions using an implicit formulation of the lattice Boltzmann method. J. Fluid Mech. 452, 61–96.
Schierholz, E.L., Gulliver, J.S., Wilhelms, S.C., Henneman, H.E., 2006. Gas transfer from air diffusers. Water Res. 40, 1018–1026.
Senhaji, R., 1993. Qualification globale du fractionnement d'une phase disperseé de faible viscosité en fonction des propriétés turbulentes de l'écoulement externe, Thesis, Ecole Centrale de Nantes.
Sevik, M., Park, S.H., 1973. The splitting of drops and bubbles by turbulent fluid flow. J. Fluids Eng. 95, 53–60.
Simonnet, M., Gentric, C., Olmos, E., Midoux, N., 2007. Experimental determination of the drag coefficient in a swarm of bubbles. Chem. Eng. Sci. 62, 858–866.
Socolofsky, S.A., 2001. Laboratory experiments of multi-phase plumes in stratification and crossflow, Ph.D. Thesis, MIT, Massachusetts, 233p.
Sun, T.Y., Faeth, G.M., 1986a. Structure of turbulent bubbly jets – I. Methods and centerline properties. Int. J. Multiphase Flow 12, 99–114.
Sun, T.Y., Faeth, G.M., 1986b. Structure of turbulent bubbly jets – II. Phase property profiles. Int. J. Multiphase Flow 12, 115–126.
Turner, J.S., 1986. Turbulent entrainment: the development of the entrainment assumption, and its application to geophysical flows. J. Fluid Mech. 173, 431–471.
Uberoi, M., Freymuth, P., 1970. Turbulent energy balance and spectra of the axisymmetric wake. Phys. Fluids 13, 2205–2210.